



## RESEARCH LETTER

10.1029/2018GL079286

### Key Points:

- A method is developed to constrain aerosol vertical profiles in the boundary layer using hyperspectral measurements of oxygen absorption
- The method is tested using hyperspectral measurement of reflected solar radiation from a mountaintop instrument to infer aerosol profiles
- The method can potentially be applied to satellite observations to constrain aerosol vertical structure on a global scale

### Supporting Information:

- Supporting Information S1

### Correspondence to:

Z.-C. Zeng,  
zcz@gps.caltech.edu

### Citation:

Zeng, Z.-C., Natraj, V., Xu, F., Pongetti, T. J., Shia, R.-L., Kort, E. A., et al. (2018). Constraining aerosol vertical profile in the boundary layer using hyperspectral measurements of oxygen absorption. *Geophysical Research Letters*, 45, 10,772–10,780. <https://doi.org/10.1029/2018GL079286>

Received 20 JUN 2018

Accepted 23 SEP 2018

Accepted article online 27 SEP 2018

Published online 12 OCT 2018

## Constraining Aerosol Vertical Profile in the Boundary Layer Using Hyperspectral Measurements of Oxygen Absorption

Zhao-Cheng Zeng<sup>1</sup> , Vijay Natraj<sup>2</sup> , Feng Xu<sup>2</sup> , Thomas J. Pongetti<sup>2</sup>, Run-Lie Shia<sup>1</sup> , Eric A. Kort<sup>3</sup> , Geoffrey C. Toon<sup>2</sup> , Stanley P. Sander<sup>2</sup> , and Yuk L. Yung<sup>1,2</sup>

<sup>1</sup>Division of Geological and Planetary Sciences, California Institute of Technology, Pasadena, CA, USA, <sup>2</sup>Jet Propulsion Laboratory, California Institute of Technology, Pasadena, CA, USA, <sup>3</sup>Department of Climate and Space Sciences and Engineering, University of Michigan, Ann Arbor, MI, USA

**Abstract** This study attempts to infer aerosol vertical structure in the urban boundary layer using passive hyperspectral measurements. A spectral sorting technique is developed to retrieve total aerosol optical depth (AOD) and effective aerosol layer height (ALH) from hyperspectral measurements in the 1.27- $\mu\text{m}$  oxygen absorption band by the mountaintop Fourier Transform Spectrometer at the California Laboratory for Atmospheric Remote Sensing instrument (1,673 m above sea level) overlooking the LA basin. Comparison to AOD measurements from Aerosol Robotic Network and aerosol backscatter profile measurements from a Mini MicroPulse Lidar shows agreement, with coefficients of determination ( $r^2$ ) of 0.74 for AOD and 0.57 for effective ALH. On average, the AOD retrieval has an error of 24.9% and root-mean-square error of 0.013, while the effective ALH retrieval has an error of 7.8% and root-mean-square error of 67.01 m. The proposed method can potentially be applied to existing and future satellite missions with hyperspectral oxygen measurements to constrain aerosol vertical distribution on a global scale.

**Plain Language Summary** Satellite and ground-based measurements have enabled accurate and continuous monitoring of total aerosol loading. However, these measurements provide little or no information on the vertical distribution of aerosols. In particular, there is poor measurement of aerosols in the planetary boundary layer, the part of the atmosphere closest to the surface. In this study, we develop an algorithm to retrieve the vertical structure of aerosols in the boundary layer using remote sensing observations of oxygen absorption with high spectral resolution. The algorithm is applied to infer the vertical profile of air pollutants in the Los Angeles basin using measurements made by a mountaintop instrument overlooking the basin. The proposed retrieval algorithm can potentially be applied to existing and future satellite missions with hyperspectral oxygen measurements to constrain the aerosol vertical distribution on a global scale. This important piece of information on aerosol vertical structure will potentially address several key priorities in the 2017 U.S. National Research Council Earth Science Decadal Survey, from forecasting air pollution in cities, quantifying the aerosol impact on Earth's climate, and reducing biases in greenhouse gas retrievals.

## 1. Introduction

Information about the global abundance, properties, and height distribution of aerosols is needed to quantify their influence on the Earth's climate and to better validate climate models, (Intergovernmental Panel on Climate Change, 2013). In addition, the health effects from pollution are the largest environmental risk (Liu & Diner, 2017). Aerosols also affect greenhouse gas retrievals from space by influencing the path of atmospheric radiation (see, e.g., Butz et al., 2009; Kuang et al., 2002; O'Dell et al., 2012). Aerosols also affect fluorescence retrievals performed in  $\text{O}_2$  absorption bands (Frankenberg et al., 2011). Aerosols, including those that contribute to poor air quality, are produced primarily within the planetary boundary layer (PBL), which is the bottom layer of the atmosphere and couples the Earth's surface and the atmosphere above. However, this near-surface layer is relatively poorly modeled, including the air pollutants trapped within this mixing layer. Improving our understanding of the PBL processes is critical to model the coupling mechanisms between the atmosphere and land in the integrated Earth system. Moreover, more accurate representation of the PBL processes related to aerosol horizontal and vertical distributions and composition can improve modeling of cloud formation and atmospheric radiative transfer (RT; Zarzycki & Bond, 2010).

Column measurements of aerosol optical depth (AOD) have been accurately and continuously observed by satellites such as Moderate Resolution Imaging Spectroradiometer (Kahn et al., 2007) and Multiangle Imaging Spectroradiometer (Diner et al., 1998) and by ground-based measurements from Aerosol Robotic Network (AERONET; Holben et al., 1998). These measurements provide little or no information on the vertical distribution of aerosols. Lidar measurements (Winker et al., 2009) have proven helpful in providing information that locates aerosol layers using active remote sensing. However, lidar instruments have a narrow swath, and it is therefore very difficult to obtain a global coverage. It has long been recognized that passive remote sensing using absorption spectroscopy of molecular oxygen has the potential for aerosol vertical profiling (Hou et al., 2017; Yamamoto & Wark, 1961). Absorption in the center of strong O<sub>2</sub> lines is saturated, such that any radiance measured in these regions must originate from scattering in the upper part of the atmosphere. In weak lines light can penetrate to lower atmospheric layers, allowing for the quantification of aerosols and other scatterers near the surface. This passive technique has been used to study cloud top height and cloud thickness (Heidinger & Stephens, 2000; O'Brien & Mitchell, 1992; Richardson et al., 2017; Yamamoto & Wark, 1961) and to investigate its potential for aerosol profiling using theoretical studies (Colosimo et al., 2016; Davis et al., 2017; Gabella et al., 1999; Geddes & Bösch, 2015; Hollstein & Fischer, 2014; Timofeyev et al., 1995) and broadband oxygen measurements from Scanning Imaging Absorption Spectrometer for Atmospheric Chartography (Sanghavi et al., 2012), Deep Space Climate Observatory (DSCOVR) (F. Xu, van Harten, et al., 2017; X. Xu, Wang, et al., 2017), POLarization and Directionality of the Earth's Reflectances (POLDER), and Medium Resolution Imaging Spectrometer (MERIS) (Dubuisson et al., 2009). In addition, satellite and airborne measurements in the ultraviolet may have the potential to retrieve the absorbing aerosol layer height (ALH; Torres et al., 1998; F. Xu, van Harten, et al., 2017; X. Xu, Wang, et al., 2017). Model simulations have shown that spectrally resolved (hereafter referred to as hyperspectral) measurements in O<sub>2</sub> absorption bands have, in principle, sufficient information content for quantifying the aerosol vertical distribution and its optical and microphysical properties (Hou et al., 2017). However, very limited progress has been made using real measurements. Aerosol profiling within the boundary layer is even more challenging because resolving the aerosol profile at subkilometer scales requires accurate hyperspectral measurements, good knowledge of aerosol optical properties and compositions, and correct characterization of surface reflection.

In this study, an algorithm based on a spectral sorting technique is proposed to retrieve the total AOD and the effective ALH in the boundary layer using hyperspectral measurements in the oxygen band centered at 1.27  $\mu\text{m}$ . The algorithm is applied to measurements made by the Fourier Transform Spectrometer at the California Laboratory for Atmospheric Remote Sensing (CLARS-FTS), located on the top of Mt. Wilson (1,673 m above sea level) overlooking the LA basin.

## 2. Data

### 2.1. Observations From CLARS

The CLARS-FTS instrument is located on the top of Mt. Wilson (1,673 m above sea level) in the LA basin and offers continuous high-resolution spectral measurements in the near infrared to shortwave infrared spectral region (effectively from 4,000 to 12,000  $\text{cm}^{-1}$ ), including the oxygen  $^1\Delta$  band at 1.27  $\mu\text{m}$ . As shown in Figure S1 in the supporting information, CLARS has two modes of operation: the Spectralon Viewing Observation mode, which quantifies the solar irradiance by measuring reflected sunlight from a Spectralon plate located immediately below the FTS telescope, and the Los Angeles Basin Survey mode, which measures reflected sunlight from surface targets in the basin. In this study, we focus on the West Pasadena surface target, as illustrated in Figure S2a. The CLARS observation geometry makes the measurements not only highly sensitive to the atmospheric composition but also very susceptible to influence by aerosol scattering and absorption due to the long light path across the boundary layer. The CLARS measurements mimic to a certain extent the off-nadir viewing of an instrument in geostationary orbit with hourly viewing capability. Details concerning the CLARS-FTS design, operation, and calibration can be found in Fu et al. (2014), K. W. Wong et al. (2015), C. K. Wong et al. (2016), and Zeng et al. (2017). High and low clouds are filtered from the CLARS data using the oxygen ratio approach (K. W. Wong et al., 2015). This study does not require the CLARS spectra to be radiometrically calibrated since only the CLARS level reflectance (the ratio of the Los Angeles Basin Survey and Spectralon Viewing Observation radiances) is used, as shown in Figure S1b.

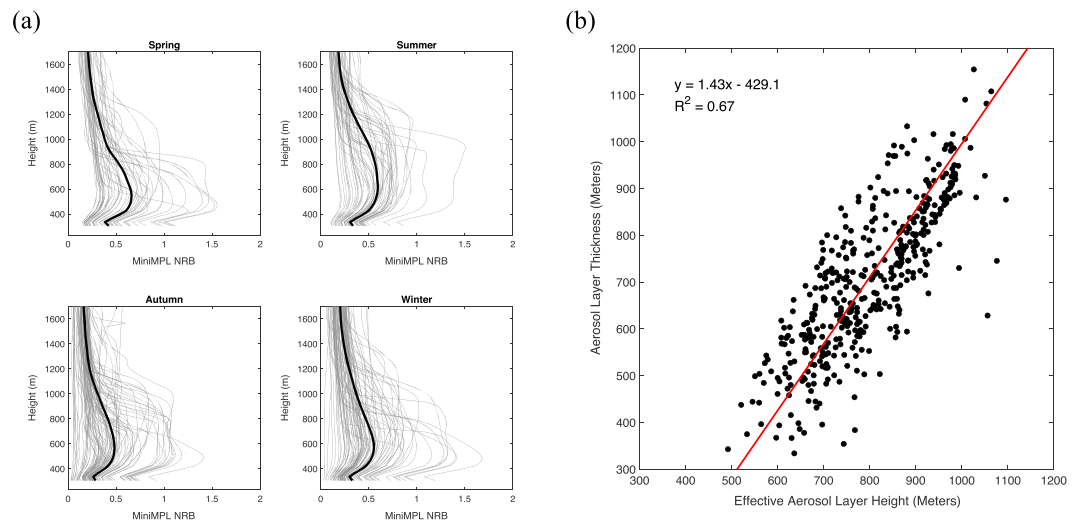


**Figure 1.** (a) Seasonal mean and variabilities of vertical profiles of normalized relative backscatter (NRB) at 2:00 p.m. measured by MiniMPL located at Caltech. The gray lines are all the available measurements from 2012 to 2014, and the bold black lines are the seasonal means. (b) Correlation between effective aerosol layer height and geometric thickness calculated using the MiniMPL measurements as shown in (a). The two parameters have a significant correlation ( $r^2 = 0.67$ ). MiniMPL = Mini MicroPulse Lidar.

## 2.2. AERONET AOD Measurements

The AERONET site at Caltech makes measurements of total AOD, from which aerosol optical properties including single scattering albedo (SSA) and phase function can be retrieved. Text S1 introduces the estimation of AOD value in the  $O_2 \ ^1\Delta$  band at  $1.27 \mu\text{m}$  using the Ångström exponent law. Figure S3 shows the seasonal histograms of AOD, SSA, and asymmetry parameter from the aerosol scattering phase function obtained from AERONET-Caltech from 2011 to 2017.

## 2.3. MiniMPL Aerosol Backscatter Measurements

The Mini MicroPulse Lidar (MiniMPL) instrument, located at Caltech, measures the aerosol backscattering at different altitudes by emitting 532-nm laser light and determining the distance to scattering events using the time of light travel (Ware et al., 2016). The raw event count reported by the MiniMPL at a vertical resolution of 30 m must be calibrated and normalized in order to arrive at the quantity of interest, viz, normalized relative backscatter (NRB), which is approximately proportional to the concentration of scatterers at a given distance above the instrument. Measurement data from 2012 to 2014 are used in this study. Figure 1a shows the seasonal mean and variabilities of vertical profiles of NRB at 2:00 p.m. The aerosol layer in the summer is relatively high mainly due to the expanded boundary layer. The calculation of effective ALH is introduced in Text S2. As a measure of the aerosol vertical expansion, the geometric thickness of the aerosol layer in this study is defined as the ratio of the integrated total NRB over all different levels to the maximum NRB. It is physically correlated with effective ALH driven by the expansion and collapse of the PBL. As shown in Figure 1b, these two data have a significant correlation in the boundary layer ( $r^2 = 0.67$ ). This correlation can be used to construct the vertical profile together with retrieved total AOD and effective ALH in the boundary layer.

## 3. Retrieval of Aerosol Vertical Profile

### 3.1. Sensitivity Study and Spectral Sorting

To understand the impact of aerosol vertical structure on the radiance observed by CLARS, a forward RT simulation is performed using the 2S-ESS RT model (Spurr & Natraj, 2011; Zeng et al., 2017; Zhang et al., 2015). The RT model settings are described in Text S3. Figure 2a shows the aerosol layer structures in the RT model. Five aerosol layers are constructed by equally dividing the height from the surface (292 m for West Pasadena surface target) to the CLARS elevation (1,673 m). The layers are centered at 430, 706,

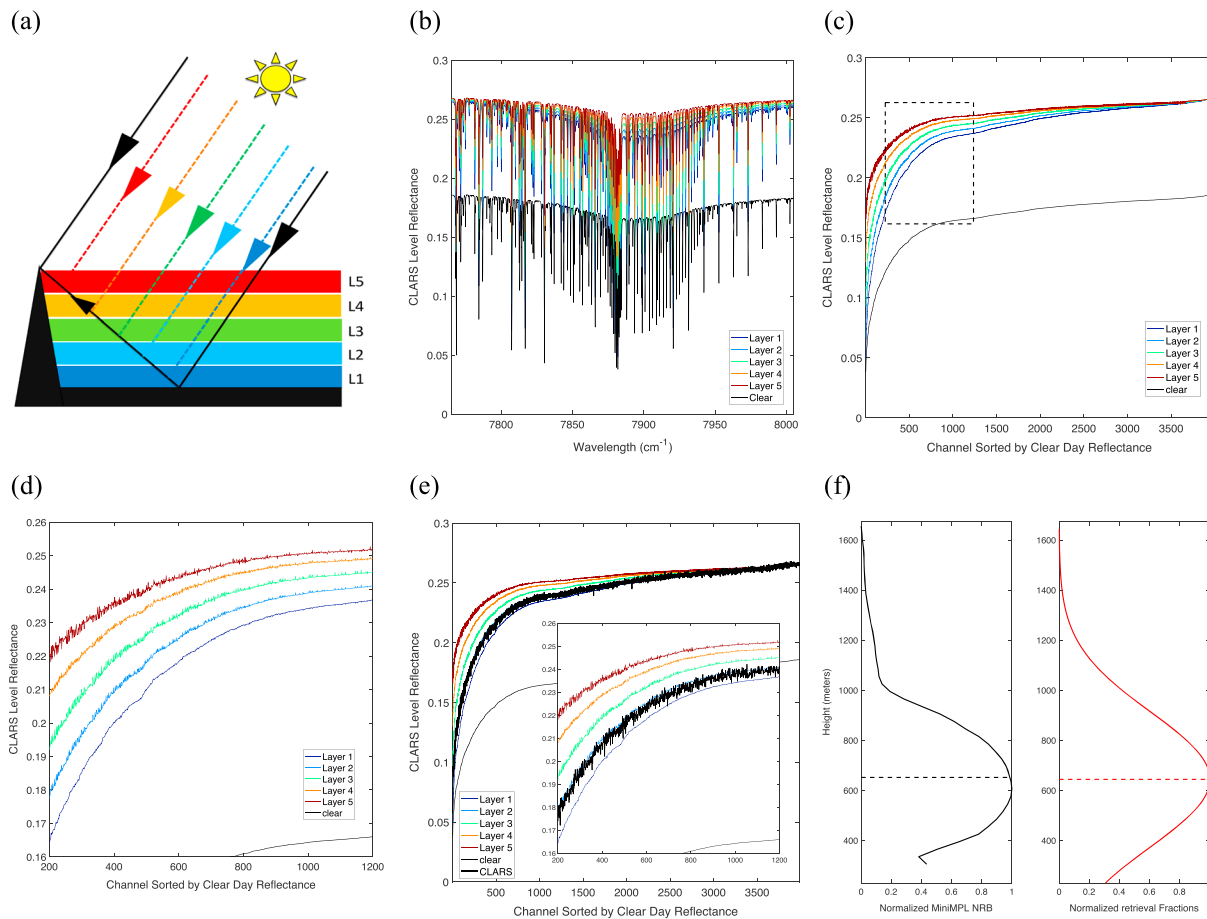


**Figure 2.** (a) Aerosol layer structures formulated in the radiative transfer model. Five aerosol layers are constructed by equally dividing the height from the surface (292 m above sea level for West Pasadena surface target) to the CLARS elevation (1,673 m). The layers are centered at 430, 706, 983, 1,259, and 1,535 m, respectively, with layer vertical thickness of 276 m. (b) Five aerosol layer scenarios simulated by adding the same amount of aerosol loading but in different layers. The simulated CLARS reflectance in the oxygen band is shown for the five scenarios (in blue to red from layer 1 to layer 5, respectively), as well as the clean scenario (in black). These simulations use the solar geometries at 14:00 on 17 September 2013, and collocated aerosol optical properties (single scattering albedo and phase function) from Aerosol Robotic Network. The solar zenith angle is 46.56°, and the aerosol scattering angle is 50.64°. (c) The simulated spectra from (b) sorted according to the reflectance value. The sorting order is obtained from the clear scenario spectra and then applied to all other scenarios. (d) Zoomed in plot of the rectangle shown in (c). (e) Same as (c) but overlaid with measured reflectance from CLARS. (f) Observed aerosol layer profile from MiniMPL and ALH (652 m) in the left panel, and the retrieved profile and ALH (644 m) in the right panel. The measured AOD (0.0257) and retrieved AOD (0.0279) at 1.27  $\mu\text{m}$  are also indicated. The corresponding AOD at 0.5  $\mu\text{m}$  is about 0.10. The MiniMPL measurements are not available below 275 m above sea level, which is the height of the building where the instrument is located. CLARS = California Laboratory for Atmospheric Remote Sensing; NRB = normalized relative backscatter; ALH = aerosol layer height; AOD = aerosol optical depth; MiniMPL = Mini MicroPulse Lidar.

983, 1,259, and 1,535 m, respectively, with a layer vertical thickness of 276 m. The selection of five layers is limited by measurement uncertainty from CLARS to build up a lookup table for ALH retrievals as described in section 3.2. Five scenarios are simulated by adding the same amount of aerosol loading but in different layers. Figure 2b shows the simulated CLARS reflectance in the 1.27- $\mu\text{m}$  band for the five scenarios as well as the clear-sky scenario. Since the aerosol has a higher reflectivity than the surface, the observed radiances are significantly larger for the five aerosol cases than the clear-sky case. These simulations use the solar geometries at 14:00 LT in September 2013 and collocated aerosol optical properties (SSA and phase function) from AERONET. We can see that, for the different scenarios, the radiance values are similar in the continuum but different within the absorption bands, with stronger absorption when the aerosol layer is placed at a lower altitude. These differences are even more obvious when we sort the radiance, as shown in Figure 2c. This is done by sorting the reflectance from the clear-sky spectrum and then applying the same order to other scenarios with aerosol scattering. Using this approach, strong, medium, and weak lines appear on the left, middle, and right sections of each curve, respectively. There

are at least two pieces of information directly available from the spectral comparison: (1) the continuum level constrains the total AOD since  $O_2$  absorption is weak and therefore the radiance is directly related to aerosol loading along the light path given surface albedo is unchanged and (2) the reflected radiance in the intermediate absorption lines, as shown in Figures 2c and 2d, exhibits large differences among the different aerosol scenarios and therefore its variability constrains ALH. The strongest absorption lines are not used in order to avoid the associated large uncertainty in the measurement (due to saturation effects). The small wiggles in the sorted radiance are caused by the fact that wavelength dependence of the oxygen absorption coefficients is different at different altitudes, which in turn is because they vary differently with pressure and temperature. The physical basis of using oxygen to study aerosol scattering is that atmospheric aerosols scatter photons back to space and therefore reduce the chance of the photons being absorbed by the oxygen, which is almost uniformly distributed in the atmosphere. Photons scattered by higher aerosol layers undergo shorter absorption paths, thereby reducing the  $O_2$  absorption depths.

From this sensitivity study, we can see that the observed hyperspectral radiance in the oxygen band has strong sensitivities to both aerosol loading and aerosol vertical structure within the boundary layer. The spectral sorting technique provides a straightforward way to extract the information on aerosol loading and its vertical structure from the observed radiance.

### 3.2. AOD and ALH Retrievals

The retrieval is implemented in two steps. First, the total AOD is retrieved by constructing a lookup table with different aerosol loadings, as shown in Figures S5a and S5b, for the purpose of fitting the observed and simulated radiances in the continuum. Subsequently, another lookup table is built by placing aerosols in different layers and comparing the simulated spectra with observations, as shown in Figure 2e. The measurements are relatively noisy compared to model simulations, probably because the model simplifies some physical processes that are otherwise hard to capture. It is evident from the measurements that the effective height of the aerosol layer lies between the first (ALH: 430 m) and second (ALH: 706 m) layers, while being closer to the latter. A quantitative comparison between measurements and simulations is needed to get the exact effective ALH. To minimize the impact of data noise on the comparison, we fit the sorted spectra to quantify the spectral shape, as described in Text S4. Different metrics can be used to quantify the difference in reflectance between model simulations and measurements. Here we use the mean value of reflectance over this intermediate absorption window calculated by averaging all CLARS level reflectance values and build the lookup table, as shown in Figure S5d. The effective ALH from CLARS measurements is then retrieved by projecting on the lookup table. The geometric thickness of the aerosol layer can be derived from the correlation plot in Figure 1b. Assuming that the aerosol vertical distribution follows a normal distribution, we can reconstruct the aerosol vertical structure, as shown in Figure 2f, based on the retrieved total AOD, effective ALH, and the derived aerosol layer geometric thickness (see Text S5 for details). It is evident that the retrieved profile reproduces the vertical structure of the measured profile very well.

### 3.3. Assessment of Retrieval Accuracy

The retrieval accuracy of the proposed method is evaluated by applying the retrieval method to all available measurements with coincident CLARS, AERONET, and MiniMPL measurements from May 2013 to December 2014. Cases with high or low clouds are excluded using the oxygen ratio technique (K. W. Wong et al., 2015). For total AOD retrievals, 160 cases from collocated CLARS and AERONET measurements are available for this comparison, as shown in Figure 3a. The AOD ranges from 0 to 0.12 (Figure S3). Aerosol optical properties from AERONET are used in the RT model for the retrieval. The retrievals are significantly correlated with the AOD from AERONET ( $r^2 = 0.74$ ; root-mean-square error, RMSE = 0.013). The total AOD retrieval has an error of 24.9% on average compared with AERONET data. Part of the variability may be due to the fact that the light paths for AERONET and CLARS are not the same. To compare the retrieved effective ALH with MiniMPL observations, data filtering is performed to ensure the validity of the measurements from AERONET and MiniMPL. First, cases with bad AOD retrieval (Figure 3a), that is, retrieval error larger than 50% (about 10% of data involved), are not used. Second, we correlate the AERONET AOD with MiniMPL backscatter data, as shown in Figure S4. Data with difference (between AERONET and MiniMPL observations) larger than 1.5 standard deviations from the mean, as indicated by red, are not included.

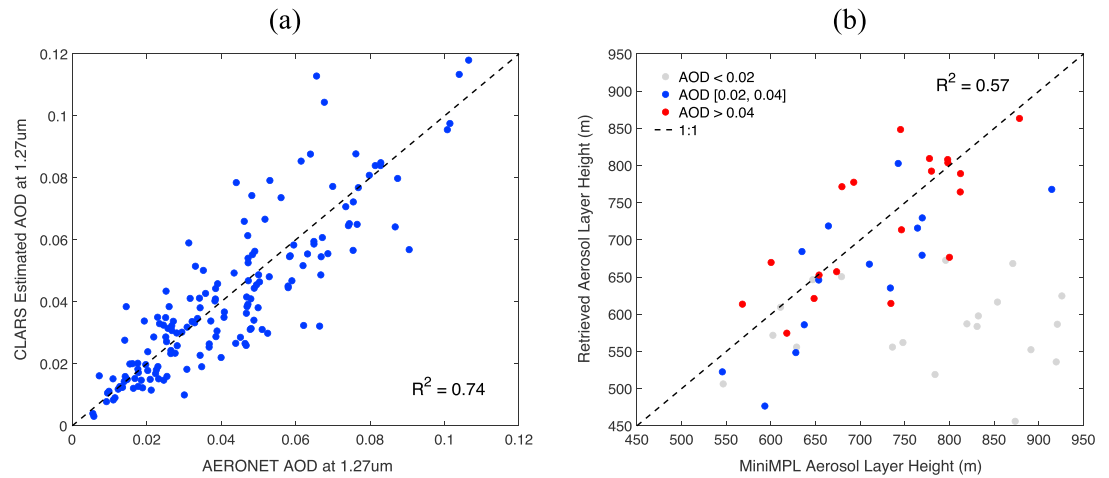


**Figure 3.** (a) Retrievals of total AOD at 14:00 from CLARS compared with corresponding AERONET-Caltech measurements. In total, 160 cases from collocated CLARS and AERONET measurements are available for this comparison. The retrievals are significantly correlated with the truth ( $r^2 = 0.74$ ; RMSE = 0.013); (b) Retrievals of effective ALH from CLARS at 14:00 compared with the corresponding aerosol layer height derived from MiniMPL at Caltech. In total, 53 cases are available from collocated CLARS, AERONET, and MiniMPL measurements. Three different levels of aerosol loading are plotted according to AOD; retrievals for AOD larger than 0.02 are significantly correlated with the truth ( $r^2 = 0.57$ ; RMSE = 67.01 m). CLARS = California Laboratory for Atmospheric Remote Sensing; AOD = aerosol optical depth; AERONET = Aerosol Robotic Network; RMSE = root-mean-square error; MiniMPL = Mini MicroPulse Lidar.

In general, these excluded cases are those days with large aerosol heterogeneity, such that the AERONET and MiniMPL data may not be representative of aerosol conditions within the CLARS light path. In total, 53 cases are available from collocated CLARS, AERONET, and MiniMPL measurements. Three different levels of aerosol loading are plotted according to AOD. We found that retrievals for AOD larger than 0.02 are significantly correlated with the truth ( $r^2 = 0.57$ ; RMSE = 67.01 m), as shown in Figure 3b. A much better performance can be found for cases with larger AOD because it provides higher aerosol scattering

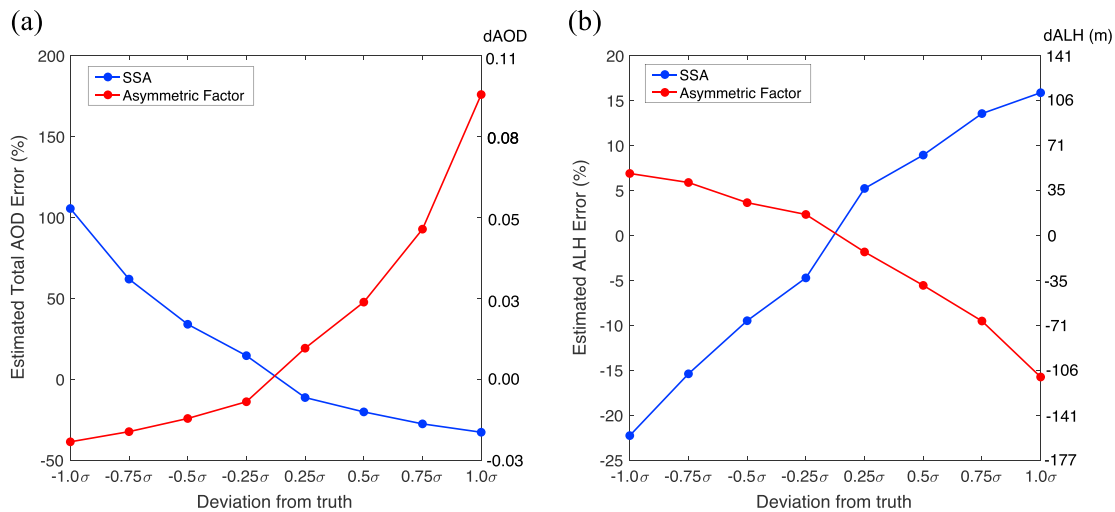


**Figure 4.** Uncertainty in total AOD and effective ALH retrievals from CLARS measurements caused by errors in input aerosol optical properties. The synthetic radiance observation is first generated using the same CLARS and solar geometries as in Figure 2, with aerosol in the middle layer (ALH = 706 m), and averaged total AOD (0.054), SSA (0.859), and asymmetry parameter (0.812) derived from long term Aerosol Robotic Network measurements at Caltech. The corresponding standard deviations ( $\sigma$ ) for SSA (0.146) and asymmetry parameter (0.0877) are used as the estimation errors. The total AOD in (a) and ALH in (b) are then retrieved by applying the proposed method to the synthetic spectral data SSA or asymmetry parameter perturbed by a certain error ( $-1.0\sigma, -0.75\sigma, -0.5\sigma, -0.25\sigma, 0.25\sigma, 0.5\sigma, 0.75\sigma, 1.0\sigma$ ). The estimation errors in total AOD and asymmetry parameter are calculated as the deviation (in percentage) from the known truth. SSA = single scattering albedo; AOD = aerosol optical depth; ALH = aerosol layer height; CLARS = California Laboratory for Atmospheric Remote Sensing.

signal that can be captured by CLARS. When aerosol loading is weak, the aerosol scattering signal may be negligible compared to that from surface reflectance. Therefore, the retrieved effective ALH tends to be smaller than the truth and closer to the surface. The AOD of 0.02 at 1.27  $\mu\text{m}$  corresponds to about 0.085 at 0.50  $\mu\text{m}$  based on the averaged Ångström coefficients that are related to the aerosol composition. The effective ALH retrieval has an error of 7.8% on average compared with the corresponding MiniMPL data. Overall, the proposed algorithm can accurately capture the variability of the total AOD and effective ALH in the PBL.

### 3.4. Impacts of SSA and Phase Function

The proposed profiling technique uses inversion products of SSA and phase function from AERONET in the study area and assumes that we have accurate estimates of these products, which may not always be the case. Here we quantify the retrieval uncertainty on total AOD and effective ALH caused by errors in the SSA and phase function. For simplicity, the aerosol scattering in the model is assumed to follow the Henyey-Greenstein type phase function (Henyey & Greenstein, 1941), which depends solely on the asymmetry parameter. The results are shown in Figure 4. As the SSA increases, the aerosols appear brighter; therefore, the estimated total AOD is lower to match the observed radiance. On the other hand, the estimated ALH increases because, for a given aerosol loading, a greater degree of scattering arises due to a shorter light path, as seen in the sensitivity study in Figure 2b. The effects of asymmetry parameter have a different pattern. As the asymmetry parameter increases, the phase function has a stronger peak in the forward direction (scattering angle less than  $20^\circ$ ) and a smaller fraction in the remaining scattering angles including the angle ( $50.64^\circ$ ) used in this simulation. In general, the error in total AOD retrieval is higher than that in ALH retrieval. As indicated by Figure 3, the RMSE in total AOD (0.013) is about 25% of the averaged total AOD (0.0541) in this simulation, while the RMSE in effective ALH (67 m) is about 10% of the true ALH (706 m). These error fractions are approximately comparable to the estimated errors due to a deviation of  $\pm 0.5\sigma$  in SSA and asymmetry parameter (Figure 4). A discussion on obtaining SSA and phase function from satellite retrievals and model simulations is provided in Text S6.

## 4. Conclusions

This work represents the first attempt to profile boundary layer aerosol vertical structure using hyperspectral remote sensing measurements. The proposed algorithm, which uses hyperspectral measurements in the 1.27- $\mu\text{m}$  oxygen absorption band to retrieve the total AOD and the effective ALH, is applied to data from the CLARS-FTS instrument, located on a mountaintop overlooking the LA basin. The effectiveness and accuracy of the retrievals are assessed by comparing with AOD from AERONET and backscatter profile from MiniMPL lidar measurements. The spectral sorting technique provides two advantages over a conventional fitting scheme: (1) information related to aerosol loading and its vertical structure can be extracted in a straightforward manner from the observed radiance and (2) the spectral region(s) with the largest sensitivity to arbitrary geophysical retrieval parameters (total AOD and ALH in this study) can be identified. The proposed retrieval algorithm to constrain aerosol vertical distribution will potentially help quantify the aerosol direct radiative forcing and reduce bias in greenhouse gas retrievals from space due to uncertainty caused by aerosol scattering.

The algorithm developed in this study has two implications for analyzing spaceborne observations, such as hyperspectral  $\text{O}_2$  A-band measurements from the OCO-2 (Crisp et al., 2012) and the upcoming OCO-3 (Eldering et al., 2013) missions. First, accuracy of ALH retrieval shows a certain dependence on SSA and phase function, whose retrieval accuracies can be further improved by combining hyperspectral oxygen absorption and polarimetric measurements in a broad spectral range (e.g., ultraviolet-near infrared of Airborne Multiangle SpectroPolarimetric Imager [Diner et al., 2005; F. Xu, van Harten, et al., 2017; X. Xu, Wang, et al., 2017] and ultraviolet-shortwave infrared of Research Scanning Polarimeter [Cairns et al., 1999; Wu et al., 2015]) to simultaneously determine aerosol profile and microphysical properties as well as surface reflection. Moreover, polarization measurements may also improve the aerosol layer detection over bright surfaces (see the discussion on surface albedo in Text S7). Second, a larger viewing angle off-nadir measurement provides more aerosol information, for example, OCO-3 off-nadir measurements with the urban target mode. In the near future, CLARS-FTS will be upgraded to include measurements in the  $\text{O}_2$  A-band at 0.76  $\mu\text{m}$ . The  $\text{O}_2$  A-band is more sensitive to scattering from fine mode aerosols while the  $\text{O}_2$   $^1\Delta$  band at 1.27  $\mu\text{m}$  is more

sensitive to scattering from coarse mode aerosols. A combination of these spectral regions may help to distinguish the profiles of fine and coarse mode aerosols.

#### Acknowledgments

We thank Jack Margolis, Chao Liu, Yuan Wang, Siteng Fan, Suniti Sanghavi, Mike Gunson, and Annmarie Eldering for stimulating discussions. V. N. acknowledges support from the NASA Earth Science US Participating Investigator program (solicitation NNH16ZDA001N-ESUSP1). F. X. acknowledges support from NASA Remote Sensing Theory program under grant 14-RST14-0100. We are also thankful for the support from the Jet Propulsion Laboratory Research and Technology Development Program. Part of the research in this study was performed at the Jet Propulsion Laboratory, California Institute of Technology, under a contract with the National Aeronautics and Space Administration. The CLARS project receives support from the California Air Resources Board and the NIST GHG and Climate Science Program. The MiniMPL was supported by the KISS Program at Caltech; data are available from the NASA Megacity project data portal: <https://megacities.jpl.nasa.gov/portal/>. AERONET data for the Caltech site are available from [https://aeronet.gsfc.nasa.gov/new\\_web/photo\\_db\\_v3/CalTech.html](https://aeronet.gsfc.nasa.gov/new_web/photo_db_v3/CalTech.html). We also thank Jochen Stutz from UCLA and his staff for their effort in establishing and maintaining the AERONET Caltech site. CLARS-FTS data are available from the authors upon request, and part of the data are available from the NASA Megacities Project at <https://megacities.jpl.nasa.gov>. We are grateful to the two anonymous reviewers whose comments helped improve the paper.

#### References

- Butz, A., Hasekamp, O. P., Frankenberg, C., & Aben, I. (2009). Retrievals of atmospheric CO<sub>2</sub> from simulated space-borne measurements of backscattered near-infrared sunlight: Accounting for aerosol effects. *Applied Optics*, 48(18), 3322–3336. <https://doi.org/10.1364/AO.48.003322>
- Cairns, B., Russell, E. E., & Travis, L. D. (1999). Research scanning polarimeter: Calibration and ground-based measurements. In *Polarization: Measurement, analysis, and remote sensing II, Proc. SPIE* (Vol. 3754, pp. 186–197). Denver, CO: International Society for Optics and Photonics. <https://doi.org/10.1117/12.366329>
- Colosimo, S. F., Natraj, V., Sander, S. P., & Stutz, J. (2016). A sensitivity study on the retrieval of aerosol vertical profiles using the oxygen A-band. *Atmospheric Measurement Techniques*, 9(4), 1889–1905. <https://doi.org/10.5194/amt-9-1889-2016>
- Crisp, D., Fisher, B. M., O'Dell, C., Frankenberg, C., Basilio, R., Bösch, H., et al. (2012). The ACOS CO<sub>2</sub> retrieval algorithm—Part II: Global XCO<sub>2</sub> data characterization. *Atmospheric Measurement Techniques*, 5(4), 687–707. <https://doi.org/10.5194/amt-5-687-2012>
- Davis, A. B., Kalashnikova, O. V., and Diner, D. J. (2017). Aerosol layer height over water from O<sub>2</sub> A-band: mono-angle hyperspectral and/or bi-spectral multi-angle observations. Preprint, <https://doi.org/10.20944/preprints201710.0055.v1>
- Diner, D. J., Beckert, J. C., Reilly, T. H., Bruegge, C. J., Conel, J. E., & Kahn, R. A. (1998). Multi-angle Imaging SpectroRadiometer (MISR) instrument description and experiment overview. *IEEE Transactions on Geoscience and Remote Sensing*, 36(4), 1072–1087. <https://doi.org/10.1109/36.700992>
- Diner, D. J., Braswell, B. H., Davies, R., Gobron, N., Hu, J., Jin, Y., et al. (2005). The value of multiangle measurements for retrieving structurally and radiatively consistent properties of clouds, aerosols, and surfaces. *Remote Sensing of Environment*, 97(4), 495–518. <https://doi.org/10.1016/j.rse.2005.06.006>
- Ding, S., Wang, J., & Xu, X. (2016). Polarimetric remote sensing in oxygen A and B bands: Sensitivity study and information content analysis for vertical profile of aerosols. *Atmospheric Measurement Techniques*, 9(5), 2077–2092. <https://doi.org/10.5194/amt-9-2077-2016>
- Dubuisson, P., Frouin, R., Dessailly, D., Duforêt, L., Léon, J.-F., Voss, K., & Antoine, D. (2009). Estimating the altitude of aerosol plumes over the ocean from reflectance ratio measurements in the O<sub>2</sub> A-band. *Remote Sensing of Environment*, 113(9), 1899–1911. <https://doi.org/10.1016/j.rse.2009.04.018>
- Eldering, A., Kaki, S., Crisp, D., & Gunson, M. R. (2013). The OCO-3 mission. Abstracts A21G-0134 presented at 2013 Fall Meeting, American Geophysical Union, San Francisco, CA, 9–13 Dec.
- Frankenberg, C., Butz, A., & Toon, G. C. (2011). Disentangling chlorophyll fluorescence from atmospheric scattering effects in O<sub>2</sub> A-band spectra of reflected sun-light. *Geophysical Research Letters*, 38, L03801. <https://doi.org/10.1029/2010GL045896>
- Fu, D., Pongetti, T. J., Blavier, J.-F. L., Crawford, T. J., Manatt, K. S., Toon, G. C., et al. (2014). Near-infrared remote sensing of Los Angeles trace gas distributions from a mountaintop site. *Atmospheric Measurement Techniques*, 7(3), 713–729. <https://doi.org/10.5194/amt-7-713-2014>
- Gabella, M., Kisselev, V., & Perona, G. (1999). Retrieval of aerosol profile variations from reflected radiation in the oxygen absorption A band. *Applied Optics*, 38(15), 3190–3195. <https://doi.org/10.1364/AO.38.003190>
- Geddes, A., & Bösch, H. (2015). Tropospheric aerosol profile information from high-resolution oxygen A-band measurements from space. *Atmospheric Measurement Techniques*, 8(2), 859–874. <https://doi.org/10.5194/amt-8-859-2015>
- Heidinger, A., & Stephens, G. L. (2000). Molecular line absorption in a scattering atmosphere, Part II: Application to remote sensing in the O<sub>2</sub> A-band. *Journal of the Atmospheric Sciences*, 57(10), 1615–1634. <https://doi.org/10.1175/1520-0469>
- Heney, L. G., & Greenstein, J. L. (1941). Diffuse radiation in the galaxy. *The Astrophysical Journal*, 93, 70–83.
- Holben, B. N., Eck, T. F., Slutsker, I., Tanre, D., Buis, J. P., & Setzer, A. (1998). AERONET—A federated instrument network and data archive for aerosol characterization. *Remote Sensing of Environment*, 66(1–16), 1998.
- Hollstein, A., & Fischer, J. (2014). Retrieving aerosol height from the oxygen A band: A fast forward operator and sensitivity study concerning spectral resolution, instrumental noise, and surface inhomogeneity. *Atmospheric Measurement Techniques*, 7(5), 1429–1441. <https://doi.org/10.5194/amt-7-1429-2014>
- Hou, W., Wang, J., Xu, X., & Reid, J. S. (2017). An algorithm for hyperspectral remote sensing of aerosols: 2. Information content analysis for aerosol parameters and principal components of surface spectra. *Journal of Quantitative Spectroscopy & Radiative Transfer*, 192, 14–29. <https://doi.org/10.1016/j.jqsrt.2017.01.041>
- Intergovernmental Panel on Climate Change (2013). In T. F. Stocker, et al. (Eds.), *Climate change 2013: The Physical Science Basis. Contribution of Working Group I to the Fifth Assessment Report of the Intergovernmental Panel on Climate Change* (pp. 595–605). Cambridge, UK, and New York: Cambridge University Press. <https://doi.org/10.1017/CBO9781107415324>
- Irion, F. W., Gunson, M. R., Toon, G. C., Chang, A. Y., Eldering, A., Mahieu, E., et al. (2002). Atmospheric Trace Molecule Spectroscopy (ATMOS) experiment version 3 data retrievals. *Applied Optics*, 41(33), 6968–6979. <https://doi.org/10.1364/AO.41.006968>
- Jethva, H., Torres, O., & Ahn, C. (2014). Global assessment of OMI aerosol single-scattering albedo using ground-based AERONET inversion. *Journal of Geophysical Research: Atmospheres*, 119, 9020–9040. <https://doi.org/10.1002/2014JD021672>
- Kahn, R. A., Garay, M. J., Nelson, D. L., Yau, K. K., Bull, M. A., Gaitley, B. J., et al. (2007). Satellite-derived aerosol optical depth over dark water from MISR and MODIS: Comparisons with AERONET and implications for climatological studies. *Journal of Geophysical Research*, 112, D18205. <https://doi.org/10.1029/2006JD008175>
- Kalnay, E., Kanamitsu, M., Kistler, R., Collins, W., Deaven, D., Gandin, L., et al. (1996). The NCEP/NCAR 40-year reanalysis project. *Bulletin of the American Meteorological Society*, 77(3), 437–471. [https://doi.org/10.1175/1520-0477\(1996\)077<0437:TNYRP>2.0.CO;2](https://doi.org/10.1175/1520-0477(1996)077<0437:TNYRP>2.0.CO;2)
- Kinne, S., Lohmann, U., Feichter, J., Schulz, M., Timmreck, C., Ghan, S., et al. (2003). Monthly averages of aerosol properties: A global comparison among models, satellite data, and AERONET ground data. *Journal of Geophysical Research*, 108(D20), 4634. <https://doi.org/10.1029/2001JD001253>
- Koffi, B., Schulz, M., Bréon, F. M., Griesfeller, J., Winker, D., Balkanski, Y., et al. (2012). Application of the CALIOP layer product to evaluate the vertical distribution of aerosols estimated by global models: AeroCom phase I results. *Journal of Geophysical Research*, 117, D10201. <https://doi.org/10.1029/2011JD016858>
- Kuang, Z. M., Margolis, J., Toon, G., Crisp, D., & Yung, Y. L. (2002). Spaceborne measurements of atmospheric CO<sub>2</sub> by high-resolution NIR spectrometry of reflected sunlight: An introductory study. *Geophysical Research Letters*, 29(15), 1716. <https://doi.org/10.1029/2001GL014298>



- Liu, Y., & Diner, D. J. (2017). Multi-angle imager for aerosols: A satellite investigation to benefit public health. *Public Health Reports*, 132(1), 14–17. <https://doi.org/10.1177/0033354916679983>
- O'Brien, D. M., & Mitchell, R. M. (1992). Error estimates for retrieval of cloud-top pressure using absorption in the A-band of oxygen. *Journal of Applied Meteorology*, 31(10), 1179–1192. [https://doi.org/10.1175/1520-0450\(1992\)031<1179:EEFROC>2.0.CO;2](https://doi.org/10.1175/1520-0450(1992)031<1179:EEFROC>2.0.CO;2)
- O'Dell, C. W., Connor, B., Bösch, H., O'Brien, D., Frankenberg, C., Castano, R., et al. (2012). The ACOS CO<sub>2</sub> retrieval algorithm—Part 1: Description and validation against synthetic observations. *Atmospheric Measurement Techniques*, 5, 99–121. <https://doi.org/10.5194/amt-5-99-2012>
- Richardson, M., McDuffie, J., Stephens, G. L., Cronk, H. Q., & Taylor, T. E. (2017). The OCO-2 oxygen A-band response to liquid marine cloud properties from CALIPSO and MODIS. *Journal of Geophysical Research: Atmospheres*, 122, 8255–8275. <https://doi.org/10.1002/2017JD026561>
- Sanghavi, S., Martonchik, J. V., Landgraf, J., & Platt, U. (2012). Retrieval of aerosol optical depth and vertical distribution using O<sub>2</sub> A- and B-band SCIAMACHY observations over Kanpur: A case study. *Atmospheric Measurement Techniques*, 5(5), 1099–1119. <https://doi.org/10.5194/amt-5-1099-2012>
- Seinfeld, J., & Pandis, S. (2006). *Atmospheric chemistry and physics: From air pollution to climate change* (p. 1224). New Jersey: John Wiley.
- Sen, B., Toon, G. C., Blavier, J.-F., Fleming, E. L., & Jackman, C. H. (1996). Balloon-borne observations of mid-latitude fluorine abundance. *Journal of Geophysical Research*, 101(D4), 9045–9054. <https://doi.org/10.1029/96JD00227>
- Spurr, R. J. D., & Natraj, V. (2011). A linearized 2-stream radiative transfer code for fast approximation of multiple-scatter fields. *Journal of Quantitative Spectroscopy & Radiative Transfer*, 112(16), 2630–2637. <https://doi.org/10.1016/j.jqsrt.2011.06.014>
- Timofeyev, Y. M., Vasilyev, A. V., & Rozanov, V. V. (1995). Information content of the spectral measurements of the 0.76 μm O<sub>2</sub> outgoing radiation with respect to the vertical aerosol optical properties. *Advances in Space Research*, 16(10), 91–94. [https://doi.org/10.1016/0273-1177\(95\)00385-R](https://doi.org/10.1016/0273-1177(95)00385-R)
- Torres, O., Bhartia, P. K., Herman, J. R., Ahmad, Z., & Gleason, J. (1998). Derivation of aerosol properties from satellite measurements of backscattered ultraviolet radiation: Theoretical basis. *Journal of Geophysical Research*, 103(D14), 17,099–17,110.
- Wang, J., Xu, X., Ding, S., Zeng, J., Spurr, R., Liu, X., et al. (2014). A numerical testbed for remote sensing of aerosols, and its demonstration for evaluating retrieval synergy from a geostationary satellite constellation of GEO-CAPE and GOES-R. *Journal of Quantitative Spectroscopy & Radiative Transfer*, 146, 510–528. <https://doi.org/10.1016/j.jqsrt.2014.03.020>
- Ware, J., Kort, E. A., DeCola, P., & Duren, R. (2016). Aerosol lidar observations of atmospheric mixing in Los Angeles: Climatology and implications for greenhouse gas observations. *Journal of Geophysical Research: Atmospheres*, 121, 9862–9878. <https://doi.org/10.1002/2016JD024953>
- Winker, D. M., Vaughan, M. A., Omar, A., Hu, Y., Powell, K. A., Liu, Z., et al. (2009). Overview of the CALIPSO mission and CALIOP data processing algorithms. *Journal of Atmospheric and Oceanic Technology*, 26(11), 2310–2323. <https://doi.org/10.1175/2009JTECHA1281.1>
- Wong, C. K., Pongetti, T. J., Oda, T., Rao, P., Gurney, K. R., Newman, S., et al. (2016). Monthly trends of methane emissions in Los Angeles from 2011 to 2015 inferred by CLARS-FTS observations. *Atmospheric Chemistry and Physics*, 16(20), 13,121–13,130. <https://doi.org/10.5194/acp-16-13121-2016>
- Wong, K. W., Fu, D., Pongetti, T. J., Newman, S., Kort, E. A., Duren, R., et al. (2015). Mapping CH<sub>4</sub>: CO<sub>2</sub> ratios in Los Angeles with CLARS-FTS from Mount Wilson, California. *Atmospheric Chemistry and Physics*, 15, 241–2252. <https://doi.org/10.5194/acp-15-241-2015>
- Wu, L., Hasekamp, O., van Diedenhoven, B., & Cairns, B. (2015). Aerosol retrieval from multiangle, multispectral photopolarimetric measurements: Importance of spectral range and angular resolution. *Atmospheric Measurement Techniques*, 8(6), 2625–2638. <https://doi.org/10.5194/amt-8-2625-2015>
- Wunch, D., Toon, G. C., Blavier, J.-F. L., Washenfelder, R. A., Notholt, J., Connor, B. J., et al. (2011). The total carbon column observing network. *Philosophical Transactions of the Royal Society A: Mathematical, Physical and Engineering Sciences*, 369(1943), 2087–2112. <https://doi.org/10.1098/rsta.2010.0240>
- Xi, X., Natraj, V., Shia, R. L., Luo, M., Zhang, Q., Newman, S., et al. (2015). Simulated retrievals for the remote sensing of CO<sub>2</sub>, CH<sub>4</sub>, CO, and H<sub>2</sub>O from geostationary orbit. *Atmospheric Measurement Techniques*, 8(11), 4817–4830. <https://doi.org/10.5194/amt-8-4817-2015>
- Xu, F., van Harten, G., Diner, D. J., Kalashnikova, O. V., Seidel, F. C., Bruegge, C. J., & et al. (2017). Coupled retrieval of aerosol properties and land surface reflection using the Airborne Multiangle SpectroPolarimetric Imager (AirMSPI). *Journal of Geophysical Research: Atmospheres*, 122, 7004–7026.
- Xu, X., Wang, J., Wang, Y., Zeng, J., Torres, O., Yang, Y., et al. (2017). Passive remote sensing of altitude and optical depth of dust plumes using the oxygen A and B bands: First results from EPIC/DSCOVR at Lagrange-1 point. *Geophysical Research Letters*, 44, 7544–7554. <https://doi.org/10.1002/2017GL073939>
- Yamamoto, G., & Wark, D. Q. (1961). Discussion of the letter by R.A. Hanel, Determination of cloud altitude from a satellite. *Journal of Geophysical Research*, 66(10), 3596. <https://doi.org/10.1029/JZ066i010p03596>
- Zarzycki, C. M., & Bond, T. C. (2010). How much can the vertical distribution of black carbon affect its global direct radiative forcing? *Geophysical Research Letters*, 37, L20807. <https://doi.org/10.1029/2010GL044555>
- Zeng, Z.-C., Zhang, Q., Natraj, V., Margolis, J. S., Shia, R.-L., Newman, S., et al. (2017). Aerosol scattering effects on water vapor retrievals over the Los Angeles Basin. *Atmospheric Chemistry and Physics*, 17(4), 2495–2508. <https://doi.org/10.5194/acp-17-2495-2017>
- Zhang, Q., Natraj, V., Li, K.-F., Shia, R.-L., Fu, D., Pongetti, T. J., et al. (2015). Accounting for aerosol scattering in the CLARS retrieval of column averaged CO<sub>2</sub> mixing ratios. *Journal of Geophysical Research: Atmospheres*, 120, 7205–7218. <https://doi.org/10.1002/2015JD023499>
- Zhang, Q., Shia, R.-L., Sander, S. P., & Yung, Y. L. (2016). XCO<sub>2</sub> retrieval error over deserts near critical surface albedo. *Earth and Space Science*, 3, 36–45. <https://doi.org/10.1002/2015EA000143>